ELSEVIER

International Journal of Heat and Fluid Flow 19 (1998) 573–581

International Journal of HEAT AND FLUID FLOW

Generation of longitudinal vortices in internal flows with an inclined impinging jet and enhancement of target plate heat transfer

K. Nakabe *, K. Suzuki, K. Inaoka, A. Higashio, J.S. Acton [1], W. Chen

Department of Mechanical Engineering, Kyoto University, Kyoto 606-8501, Japan

Abstract

Flow velocity measurements and heat transfer experiments were carried out for a jet obliquely discharged into a crossflow in a duct. The flow measurements were made with optical fiber laser Doppler velocimetry, and the heat transfer experiments were made by making use of a thermochromic liquid crystal. The obtained velocity data reveal that the inclined jet is effective in generating longitudinal vortices in the crossflow. It is demonstrated that the longitudinal vortices are effective in enhancing target plate jet impingement heat transfer. It is, therefore, promising as a means to effectively cool inner surfaces of high temperature gas turbine vanes. The obtained heat transfer data are discussed in detail in comparison with the measured flow field and turbulence data.

Keywords: Jet impingement; Longitudinal vortex; Heat transfer; Thermochromic liquid crystal; Turbulence

Notation

d	jet nozzle diameter
H_D	duct height
k	turbulent kinetic energy
Nu	Nusselt number
q_w	wall heat flux
Re_C	crossflow Reynolds number based on hydraulic diameter
Re_J	jet Reynolds number based on jet nozzle diameter
T_{in}	inlet fluid temperature
T_{TC}	reference temperature measured with thermocouples
T_w	target wall temperature
U, V, W	time-averaged velocity components in the x-, y- and z-directions
u, v, w	fluctuating velocity components in the x-, y- and z-directions
u', v', w'	RMS intensities of the fluctuating velocity components in the x-, y- and z-directions
U_C	time-averaged crossflow inlet velocity
VR	jet to crossflow velocity ratio
x, y, z	streamwise, normal and spanwise coordinates

Greek

α	heat transfer coefficient
θ	skew angle
λ	thermal conductivity
ϕ	pitch angle

1. Introduction

Generation of longitudinal vortices is an effective way to control the characteristics of near-wall flows and therefore to enhance the wall heat transfer (Suzuki, 1996; Suzuki et al., 1996). Its effectiveness in enhancing turbulent heat transfer has been well demonstrated both for the case where wing-type vortex generators are directly attached to a heat transfer surface (Eibeck and Eaton, 1987; Tiggelbeck et al., 1994; Fiebig, 1995) and for the case where they are attached to a Large Eddy Break-Up manipulator mounted at a position detached from a heat transfer surface (Inaoka et al., 1992; Inaoka and Suzuki, 1995).

In some practical cases, however, coolant passages are not large enough in size to mount the wing-type vortex generators. For example, this is the case of the inner cooling of a gas turbine vane. Fig. 1 schematically illustrates the configuration of the most recent vane. A duct called "insert" is mounted in the vane to feed coolant air into the inside of the vane. Jets discharged from holes drilled in the insert impinge on the inner surfaces of the vane and cool it. The clearance for coolant passage between the inner surface of the vane and the outer surface of the insert is normally less than one millimeter. Thus, it is valuable to find a way to generate longitudinal vortices without mounting any kind of vortex generators for heat transfer enhancement. The present study was initiated to investigate the possibility of intentionally generating the longitudinal vortices by making use of jets themselves for the situation where jets are accompanied with crossflow.

* Corresponding author. E-mail: nakabe@htrans.mech.kyoto-u.ac.jp.

[1] Master course student, Department of Mechanical Engineering, Queen's University, Ontario, Canada, under AIEJ (Association of International Education, Japan) short-term student exchange promotion program.

0142-727X/98/$ – see front matter
PII: S0142-727X(98)10019-X

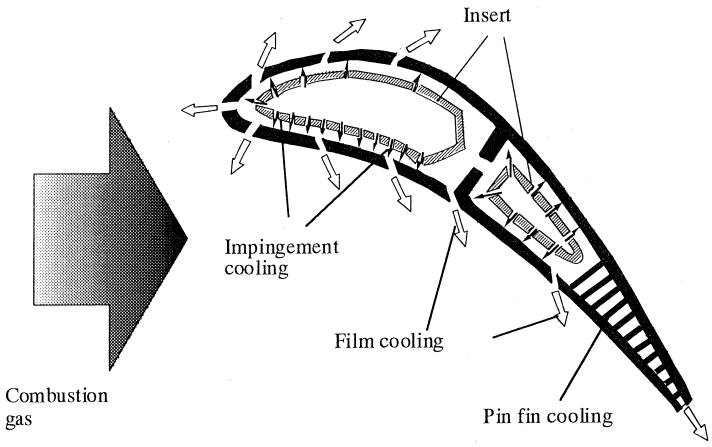

Fig. 1. Schematical illustration of gas turbine vane.

A similar attempt was made by Johnston and Nishi (1990), but their objective was to use the generated longitudinal vortices as a means to suppress flow separation from the surface of the plate installed with a jet nozzle. In the present study, it is attempted to generate the longitudinal vortices as a means to enhance heat transfer from a target plate facing to the jet nozzle.

2. Experimental apparatus, methods and conditions

Fig. 2 shows a schematic view of the experimental apparatus used in the present study. The present working fluid was water driven by the head difference between a constant head tank 1 and an outlet 10 of a test section 4. The flow supplied into the horizontally positioned test section from a contraction 3 serves as a crossflow for an impinging jet. A circular jet nozzle 12 with an oval shape open end was mounted flush with the bottom wall surface of the test section. The jet nozzle and test section were, respectively, made with brass and transparent acrylic resin.

The test section dimensions are illustrated in Fig. 3 together with some geometric parameters, the jet nozzle arrangement and the coordinate system to be used in the present study. The origin of the coordinate system is located at the center of the open end of the jet nozzle. x, y and z designate, respectively, the streamwise, normal and spanwise coordinates. The discharged jet from the nozzle impinges obliquely onto the top wall of the test section. The direction of the jet is characterized by the following two angles; one is a pitch angle ϕ raised from the bottom wall surface, and the other a skew angle θ measured between the crossflow and the direction of the impinging jet projected on a horizontal plane. The pitch and skew angles were fixed at 45° and 90°, respectively, in the present experiments. The nozzle center is located offset from the center line of the bottom wall so as to give more space on the jet-discharged side in a cross-section.

The test section was 432 mm wide and 30 mm high, and the aspect ratio was then 14.4. The jet nozzle diameter was 6 mm. Thus, the height of the test section is five times the nozzle diameter, which is regarded to be optimum in heat transfer performance of the normally impinging jet (Sparrow et al., 1975). The test section was preceded by the developing section of 2.2 m long, or 36 hydraulic diameter long, in which the crossflow comes into a fully developed state. The crossflow Reynolds number Re_C based on the time-averaged crossflow velocity at the inlet, U_C, and the hydraulic diameter of the test section were kept constantly equal to 5000. The jet to crossflow velocity ratio VR was changed in three steps, 3, 5 and 7. The values of the corresponding jet Reynolds number Re_J based on the jet velocity and the nozzle diameter were 1500, 2500 and 3500.

As has been reported previously (Nakabe et al., 1996; Nakabe et al., 1997), flow visualization was first made for laminar flow cases at a reduced crossflow velocity ($Re_C = 500$) but at the above mentioned values of the velocity ratio VR to establish a general picture of the flow pattern to be formed

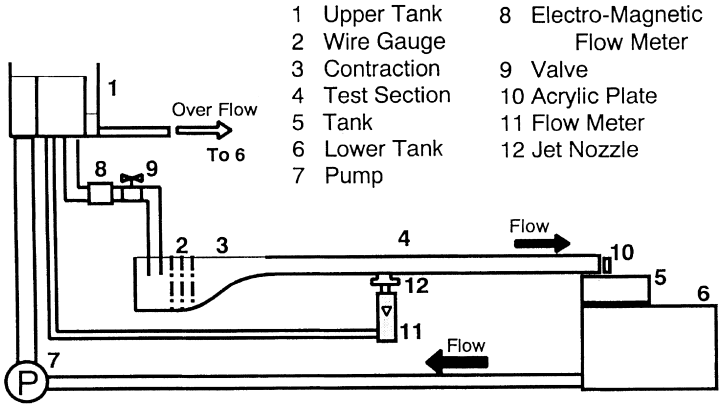

Fig. 2. Experimental apparatus.

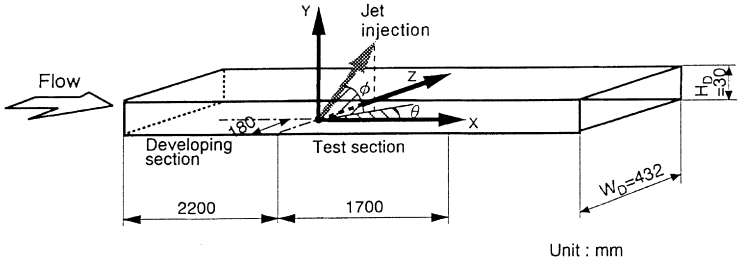

Fig. 3. Test section.

in the test section and to see if longitudinal vortices could be generated. For this purpose, particle tracking velocimetry was applied to the sequential images taken by a CCD video camera mounted to view the cross-section of the test section from its downstream end. Velocity vector maps of secondary flows were then constructed at several different stream wise locations from the jet nozzle. Information obtained from the previous studies will be referred to in the following discussion.

In the present study, flow and turbulence measurements were made quantitatively in detail with a two-color, three-beam optical fiber laser Doppler velocimeter. A 1.5 W Ar^+ laser was used as a beam source in the back-scatter mode LDV optical system, and a spheroidal measuring control volume was of the size of 115 μm in diameter and 1.44 mm in length. Scattered light was detected by photomultipliers and their output signals were converted into velocity signals by making use of a DISA phase-locked loop frequency tracker system. A Bragg-cell was used to give a frequency shift in order to make possible the measurement of backward flow velocity. The frequency was shifted back in the later stage of the signal processing into the signal proportional to actual velocity.

Heat transfer experiments were also made in addition to the flow measurements. The top plate of the test section, herein referred to as the heat transfer target plate, was almost entirely covered with smoothly glued thin, six stainless steel strips 50 mm wide and 20 μm thick as shown in Fig. 4. These strips were connected electrically in series and were heated by passing an alternating current through them. Thus, basically constant wall heat flux heating condition was established as will be explained later. The surface temperature of the target plate was measured by making use of thermochromic liquid crystals. Liquid crystal sheets were placed between the heater strips and the transparent top cover plate of the test section. Color images of the liquid crystal sheets were taken from the outside with a CCD video camera and were stored in color frame buffer memories of a workstation.

A hierarchy neural network method (Kimura et al., 1993; Matsumoto et al., 1996) was applied to convert the color images into temperature distributions on the surface of the target wall. This method is much superior, both in the spatial resolution and in the surface area to be measured, to the previous one in which the surface temperature was measured with hundreds of thermocouples attached to the back surface of the heated stainless steel strips (Nakabe et al., 1996; Acton et al., 1997). Details of the conversion method will be reported elsewhere (Nakabe et al., 1998). A comparison between the wall temperature T_w converted from the color images and the reference temperature T_{TC} directly measured with K-type thermocouples are shown in Fig. 5. Standard deviation of the difference between the two temperatures was 0.18 K in the whole range from 26.5°C to 43.5°C, and the 95% coverage for the measurement uncertainty (ANSI/AMSE, 1985) was 0.3 K.

Heat transfer coefficient α and Nusselt number Nu based on the hydraulic diameter ($=2H_D$) are defined as follows:

$$\alpha = \frac{q_w}{(T_w - T_{in})}, \quad \mathrm{Nu} = \frac{\alpha(2H_D)}{\lambda}. \tag{1}$$

T_w and T_{in} are, respectively, the local heat transfer surface temperature and the inlet flow temperature. λ is the thermal conductivity of water and H_D the height of the test section. The wall heat flux q_w was calculated from the electric power input. Heat conduction loss toward the rearside of the target plate was neglected since it was evaluated to be less than 3% of the total heat flux. Heat radiation loss from the heat transfer

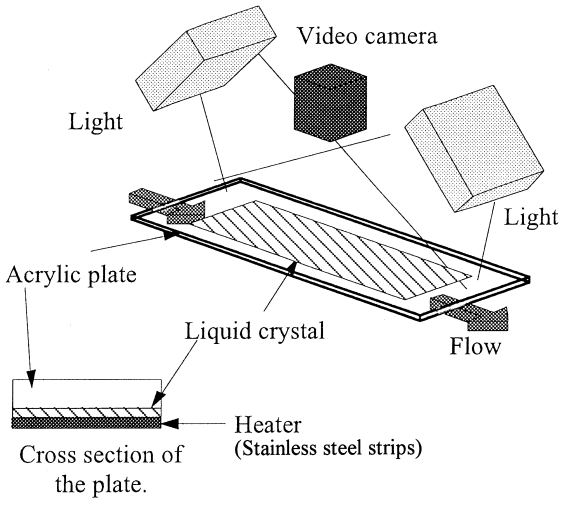

Fig. 4. Experimental apparatus for heat transfer measurements.

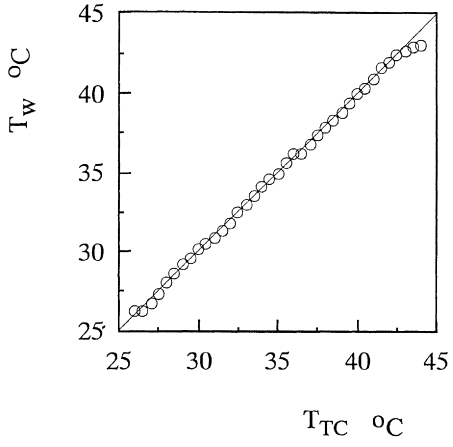

Fig. 5. T_w vs. T_{TC}.

surface was also negligibly small so that the wall surface was regarded to be heated at uniform heat flux.

3. Results and discussion

3.1. Nusselt number distributions

Fig. 6 shows examples of the contours of the local Nusselt number on the target plate for three cases of VR = 3, 5 and 7 at the constant crossflow Reynolds number, $Re_C = 5000$. The area covered ranges from $x/d = -5$ to 45 and from $z/d = -10$ to 20. Here, d is the jet nozzle diameter. Indexed gray scales drawn in the figure correspond to the values of the Nusselt numbers. It can be seen in Fig. 6(a) that the region where heat transfer enhancement was attained has a comet-like shape elongated in the x-axis direction. The conspicuously enhanced region of heat transfer, hereafter, is defined as the region where the Nusselt number takes a value larger than one hundred. The peak Nusselt number is found to appear at a position around $(x/d, z/d) = (9.0, 4.0)$. It indicates that the jet stagnation point is shifted downstream due to the effect of the crossflow and is located off the x-axis due to the oblique impingement of the jet.

For the case of higher VR value, VR = 5, shown in Fig. 6(b), the area of the conspicuously enhanced region of heat transfer expands in the positive spanwise direction and covers the region ranging from a bit below the x-axis of the test section, $z/d = -1$, to $z/d = 13$. The peak Nusselt number increases and its position is shifted back upstream to a position around $(x/d, z/d) = (6.0, 4.0)$, if compared with the above lower VR value case shown in Fig. 6(a). Further spatial expansion of the conspicuously enhanced region of heat transfer, increase of the peak Nusselt number and upstream shift of its position occur with a further increase in the VR value. The enhanced region, therefore, takes a shape like a fan a little elongated in the spanwise direction, in the case of VR = 7 as shown in Fig. 6(c). The upstream shift of the peak Nusselt number position may reflect that the jet impingement position streamwisely comes closer to $x/d = 0$ with an increase in the VR value because of relatively dominant jet penetration in the crossflow. In contrast to this, the spanwise position of the peak Nusselt number remains almost unchanged regardless of the VR value.

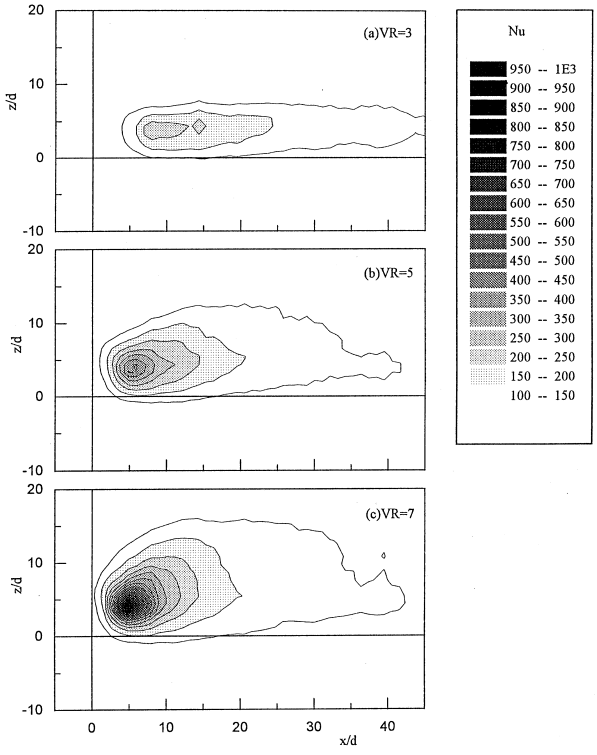

Fig. 6. Nu contours ($Re_C = 5000$).

3.2. Velocity distributions

Fig. 7(a) shows an example of the contours of the non-dimensional time-averaged value of y-direction velocity, V/U_C, measured in the middle plane between the top and bottom walls of the test section, i.e. $y/d = 2.5$, for an experimental condition corresponding to the case of Fig. 6(b), i.e. VR = 5 and $Re_C = 5000$. The dark gray and black parts in the figure represent positive velocity regions which indicate upwash flows or flows toward the target wall of the test section, while the light gray and white parts indicate negative velocity regions, that is, downwash flows or flows toward the nozzle-installed plate. As seen in this figure, strong upwash flows appear in the spanwise range of the plotted area of the middle plane approximately from $z/d = 0$ to $z/d = 5$, regardless of the streamwise distance. Downwash flows, on the other hand, appear on both sides of the upwash flow region. It, therefore, obviously reveals that a pair of counter-rotating longitudinal vortices are generated throughout the whole streamwise positions plotted in the figure. The center of a longitudinal vortex which rotates anti-clockwise, if taken as upstream view from the

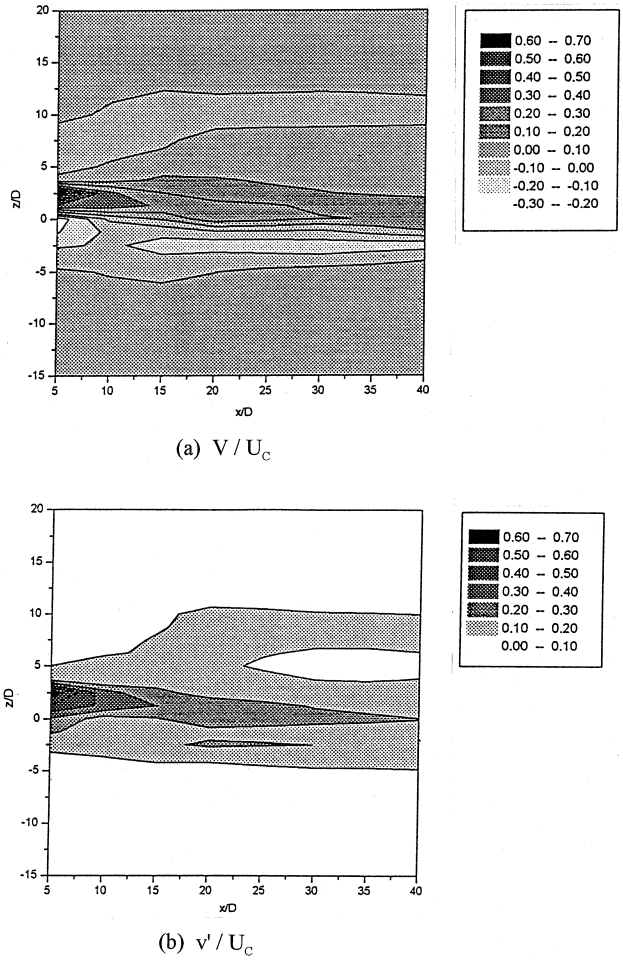

Fig. 7. V and v' contours ($y/d = 2.5$, VR = 5 and $Re_C = 5000$).

downstream end, is located approximately on the line $z/d = 0$. This anti-clockwise-rotating vortex has positive streamwise vorticity constructed from the time-averaged velocity components, V and W. The center of another relatively weaker but larger-scale clockwise-rotating longitudinal vortex is situated around $z/d = 5$ at a streamwise position just downstream the nozzle and then asymptotically approaches to a spanwise position of $z/d = 10$. Flow visualization observation, that were made for a laminar flow in the preliminary experiments (Nakabe et al., 1996), showed that the center of the latter vortex takes a similar position, and that the position moves away from the x-axis with an increase in the VR value.

The distribution of non-dimensional RMS intensity of y-direction fluctuating velocity, v'/U_C, in the middle plane between

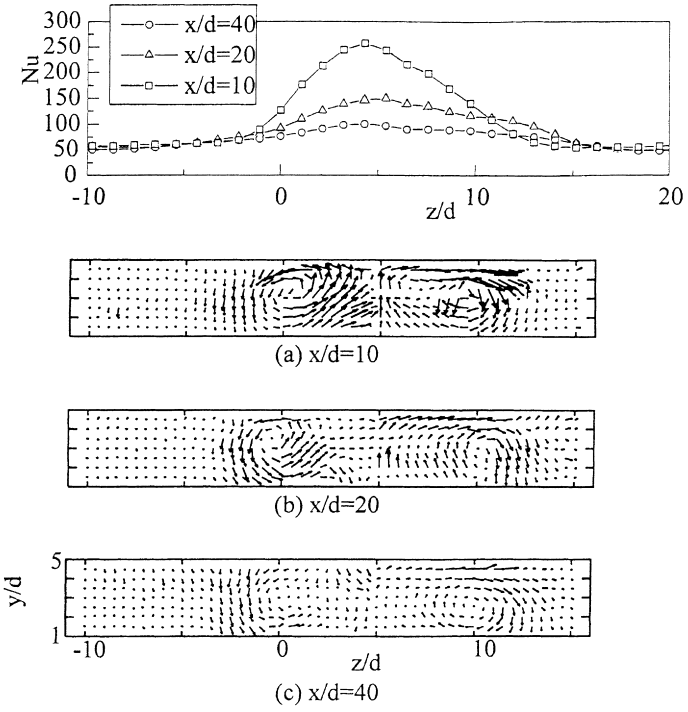

Fig. 8. Nu distributions and velocity vector maps (VR = 5 and $Re_C = 5000$).

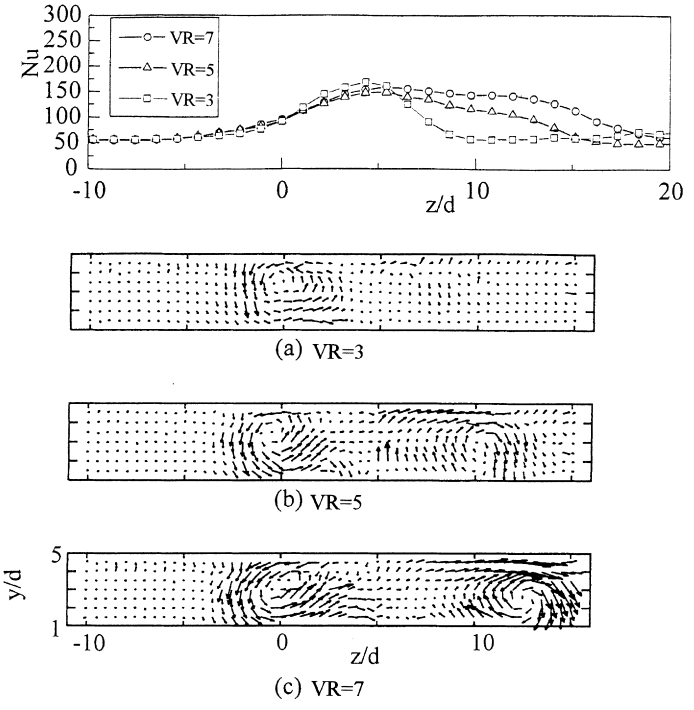

Fig. 9. Nu distributions and velocity vector maps ($x/d = 20$ and $Re_C = 5000$).

the top and bottom walls of the test section is shown in Fig. 7 (b). Indexed gray scales drawn in this figure indicate the RMS values. The high turbulence intensity region observed in the figure corresponds to the upwash flow regions induced by the inclined jet or in between a pair of counter-rotating longitudinal vortices.

3.3. Relation between flow field characteristics and heat transfer enhancement from target plate

Fig. 8 shows the spanwise distributions of Nusselt number obtained by slicing the spatial distribution shown in Fig. 6(b) for the case of VR = 5 at three different streamwise locations:

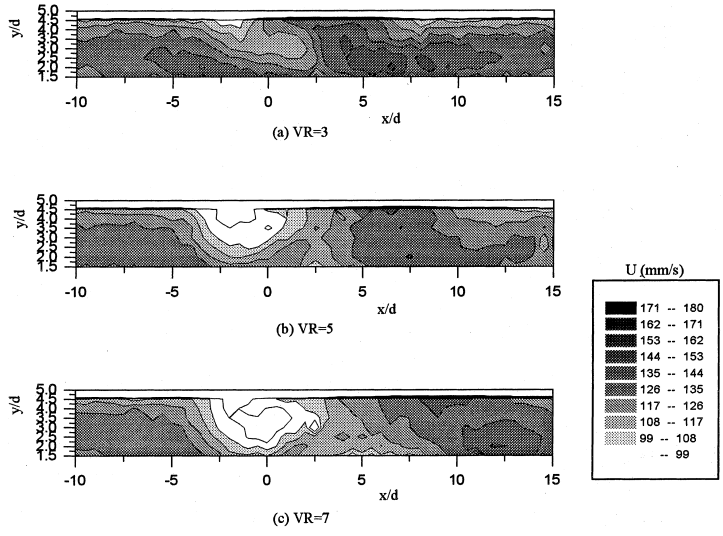

Fig. 10. U contours ($x/d = 20$ and $Re_C = 5000$).

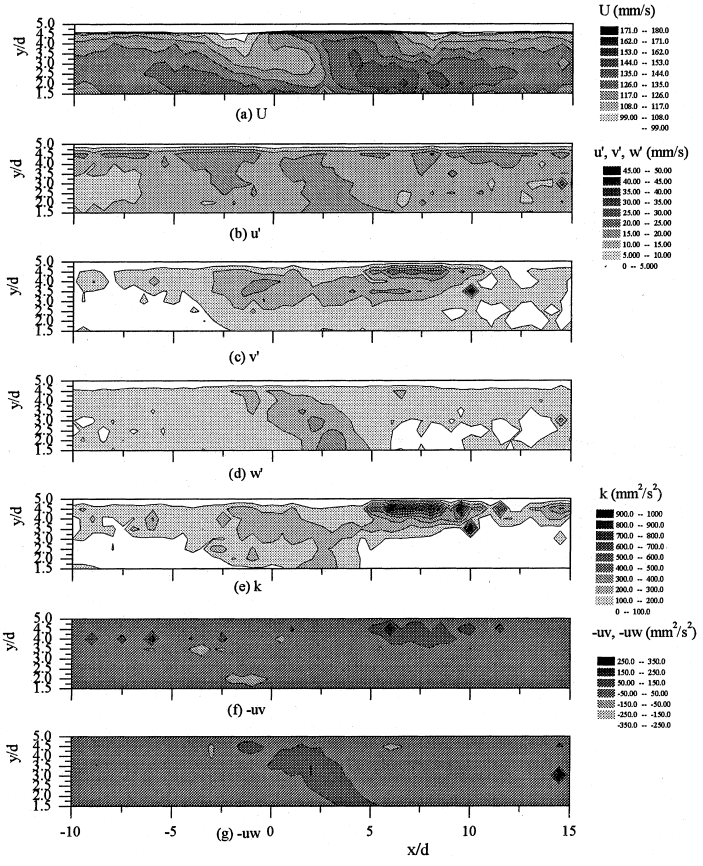

Fig. 11. Contours of turbulence components (VR = 3, $x/d = 20$ and $Re_C = 5000$).

(a) $x/d = 10$, (b) $x/d = 20$ and (c) $x/d = 40$. The secondary flow velocity vector maps for the corresponding cases are also shown for comparison. All figures of the Nusselt number distributions and the velocity vectors were drawn based on a view from the downstream end of the test section. A pair of counter-rotating longitudinal vortices mentioned in the previous section are clearly seen in the figure; one with anti-clockwise rotation is situated at an almost constant spanwise location around $z/d = 0$, and the other with clockwise rotation is shifted a little in the spanwise direction towards a position, $z/d = 10$.

Comparison between the Nusselt number distributions and the velocity vector maps shows that the enhanced region of heat transfer corresponds very well to the locations of the counter-rotating longitudinal vortices. The secondary flow velocity in the cross-section becomes smaller downstream as a whole. Following this decrease of the velocity, Nusselt number in the whole enhanced region also decreases along the streamwise direction. The right hand region of the Nusselt number distribution has gentle slopes at $x/d = 20$ and 40. The Nusselt number in this region is increasing at $x/d = 20$, and is decreasing at $x/d = 40$. Relatively large values remain from $x/d = 14$ to 25 in the right hand region of the Nusselt number distributions. These Nusselt number distribution patterns correspond to the slight spanwise movement of the clockwise-rotating vortex mentioned previously.

The spanwise positions of the peak Nusselt number are located around $z/d = 4$ which corresponds to the region of the upwash flows induced by a pair of the counter-rotating vortices. This upwash flow supplies fresh fluid or cooler fluid to the near region of the target plate and enhances the heat transfer from the target plate.

Fig. 9 compares the spanwise distributions of the Nusselt number with the secondary flow velocity vector maps for three different values of the velocity ratio, VR = 3, 5 and 7, but at the same streamwise location, $x/d = 20$. The anti-clockwise-rotating longitudinal vortex of positive streamwise vorticity is situated at almost the same position around $z/d = 0$ in all the cases. Combining this with the results of Fig. 8, a conjecture can be developed that this vortex has the same origin as the one previously studied by Johnston and Nishi (1990) near the nozzle-installed wall. They made experiments with a test section having larger size in y-direction. The other vortex having the clockwise rotation is clearly observed around $z/d = 10$ for the case of VR = 5 and also around $z/d = 13$ for the case of VR = 7, but is weakened in the case of VR = 3. The position of the rotating vortex moves away from the nozzle position in z-direction as the VR value is increased. This vortex induces strong spanwise flow sweeping the top wall surface of the test section above its center.

The spanwise position of the peak Nusselt number, noticeably observed in the case of VR = 3, is located around $z/d = 4$ which corresponds to the region of the upwash flow mainly induced by the anti-clockwise vortex. Studying the peak position of Nusselt number in a little more detailed manner, it is found to move a little toward the right side wall of the duct with an increase in the VR value. This will be discussed below again.

Compared with the case of VR = 3, the right hand region of the Nusselt number distribution becomes less steep at VR = 5 and, when VR = 7, the Nusselt number distribution exhibits a shape almost like a plateau in the wide range of the spanwise position from $z/d = 5$ to $z/d = 18$. This part of the Nu distribution corresponds to the region where the flow spanwisely

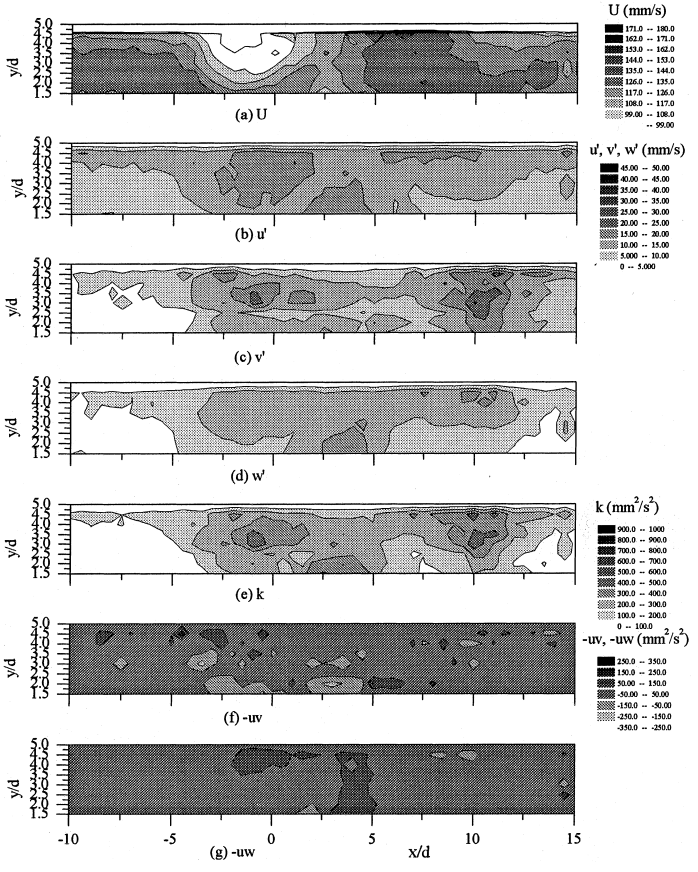

Fig. 12. Contours of turbulence components (VR = 5, $x/d = 20$ and $Re_C = 5000$).

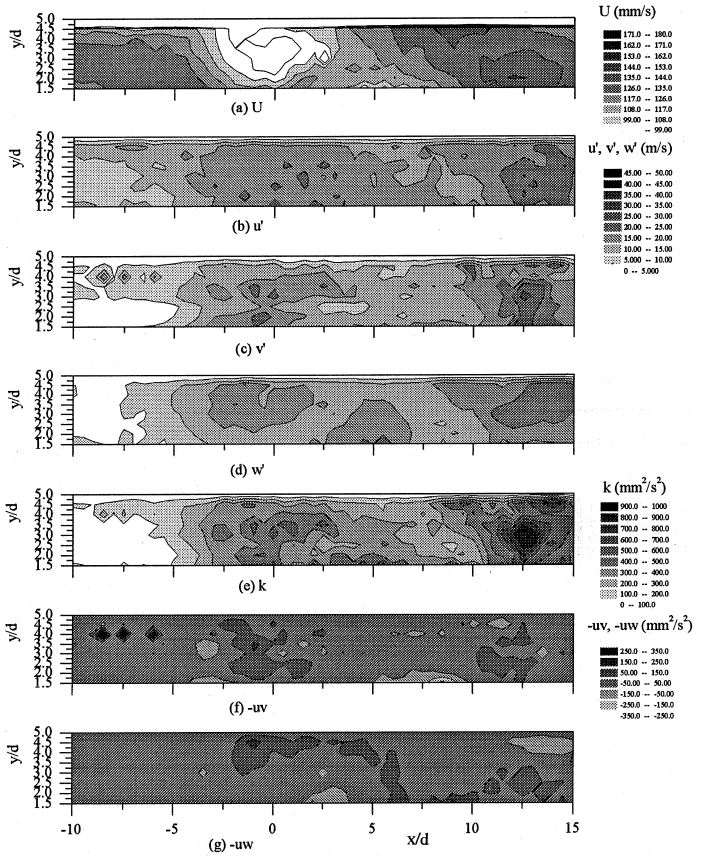

Fig. 13. Contours of turbulence components (VR = 7, $x/d = 20$ and $Re_C = 5000$).

sweeping the target plate surface appears accompanied with the generation of the clockwisely rotating vortex.

Fig. 10 shows the contours of the time-averaged streamwise velocity, U, obtained in the same cross-section plane as the one shown in Fig. 9, $x/d = 20$, for the three different cases of VR = 3, 5 and 7. Indexed gray scales correspond to the values of the velocity. In the case of VR = 3, a small low velocity region appears near the top wall surface just on the left side of $z/d = 0$. The low velocity region expands wider as the VR value is increased. The lower streamwise velocity in this region is mainly caused by the jet itself. The jet acts like a fence to the approaching flow and, thus, the velocity defect produced in its wake lasts over a long distance. Similar velocity defect accompanying the discharged jet was also observed by Compton and Johnston (1992). Slight movement of the peak Nusselt number position with an increase in the VR value pointed out in the above may be related to this expansion of the low velocity region with an increase in the VR value. Low streamwise velocity near the heat transfer surface suppresses the wall heat transfer. Then, the left side of the Nusselt number distribution becomes a little lower so that the peak Nusselt number position looks apparently moving in the right hand direction.

A more important feature observed in this figure is that a higher streamwise velocity region exists just on the left side of the center of the clockwise-rotating longitudinal vortex. This high velocity region is present very near the surface of the top wall so that this should be related to the increase of the Nusselt number on the right side of its peak; the less steep slope on the right side of the peak Nusselt number distribution in the case of VR = 5 and the plateau-like shape in the case of VR = 7 are shown in Fig. 9. Strong spanwise flows observed near the top wall shown in Fig. 9 sweep the surface of the top wall together with this high stream wise velocity flow. This should be the main cause of the heat transfer enhancement on the right-hand side region of the peak Nusselt number.

Figs. 11–13 show the distributions of the RMS velocity fluctuation intensities, turbulent kinetic energy and Reynolds stresses, u', v', w', k, $-\overline{uv}$ and $-\overline{uw}$, for the three different cases of VR = 3, 5 and 7, respectively, under the constant crossflow Reynolds number, $Re_C = 5000$, together with the streamwise velocity contours, U, already shown in Fig. 10. Indexed gray scales corresponds to each values. All contours of the RMS intensities of the velocity fluctuation components, (b) u', (c) v' and (d) w', demonstrate that the regions affected by the longitudinal vortices and/or impinging jet have large RMS values. Turbulent kinetic energy, k, in particular, has conspicuously large values in two regions corresponding very well to the positions of a pair of centers of the counter-rotating longitudinal vortices, as clearly seen in Figs. 12(e) and 13(e).

These data of the turbulence intensities should serve as a good database to examine a numerical computation of the presently discussed longitudinal vortices generated with the obliquely discharged jet into turbulent crossflow.

4. Conclusions

Flow measurements and heat transfer experiments were made for an obliquely impinging jet with a turbulent crossflow of the Reynolds number, Re_C, equal to 5000 in three different cases of the velocity ratio of the jet to crossflow, VR, equal to 3, 5 and 7. The main results obtained in the present study are shown as follows:

1. Generation of a pair of counter-rotating longitudinal vortices was clearly observed; one having anti-clockwise rotation is situated constantly around $z/d = 0$ regardless of the VR value, and the other having clockwise rotation moves away from the nozzle position in the z-direction with an increase in the VR value.
2. Heat transfer enhancement can be attained over wider span-wise region as the VR value is increased. This expansion of the region of the high Nusselt number distribution is caused by the high streamwise velocity flow combined with spanwise flows sweeping the surface of the target plate, which are produced by the clockwisely rotating longitudinal vortex.
3. The peak Nusselt number appears around $z/d = 4$–5, which is caused by the upwash region supplying fresh fluid to the near region of the target plate surface.
4. The regions of the longitudinal vortices and/or impinging jet have large values of the RMS velocity fluctuation components, u', v' and w'. Turbulent kinetic energy, k, in particular, has conspicuously large values in the regions corresponding well to the positions of a pair of the centers of the counter-rotating longitudinal vortices.

Acknowledgements

This research was partially supported by the Grant-in-Aids of Scientific Research, Ministry of Education, Science and Culture, Japan. The authors wish to express their gratitude to Messrs. Ai, T. and Hada, S., students of Kyoto University, for their cooperation in experiments.

References

Acton, J.S., Higashio, A., Inaoka, K., Nakabe, K., Suzuki, K., 1997. An experimental study on the flow and heat transfer characteristics of longitudinal vortices induced by an inclined impinging jet into across flow (Further report). In: Proceedings of First Symposium on Flow Visualization and Image Processing, vol. 2. pp. 457–462.

ANSI/AMSE, 1985. Measurement uncertainty. ASME Performance Test Codes, Supplement on Instruments and Apparatus, Part 1. PTC19.1-1985.

Compton, D.A., Johnston, J.P., 1992. Streamwise vortex production by pitched and skewed jets in a turbulent boundary layer. AIAA J. 32, 640–646.

Eibeck, P.A., Eaton, J.K., 1987. Heat transfer effects of a longitudinal vortex embedded in a turbulent boundary layer. Trans. ASME: J. Heat Transfer 109, 16–24.

Fiebig, M., 1995. Vortex generators for compact heat exchangers. J. Enhanced Heat Transfer 2, 16–24.

Inaoka, K., Suzuki, K., 1995. Structure of the turbulent boundary layer and heat transfer downstream of a vortex generator attached to a LEBU plate. In: Durst, F. et al. (Eds.), Turbulent Shear Flows, vol. 9. Springer, Berlin, pp. 365–382.

Inaoka, K., Suzuki, K., Hagiwara, Y., Suzuki, K., Suzuki, H., 1992. Heat transfer augmentation in a turbulent boundary layer disturbed by means of a vortex generator. Heat Transfer – Japanese Research 21, 721–735.

Johnston, J.P., Nishi, M., 1990. Vortex generator jets – A means for flow separation control. AIAA J. 30, 989–994.

Kimura, I., Kuroe, Y., Ozawa, M., 1993. Application of neural networks to quantitative flow visualization. J. of Flow Visualization and Image Processing 1, 261–269.

Matsumoto, R., Kikkawa, S., Senda, M., Suzuki, M., 1996. Effect of a single oblique pin fin on end wall heat transfer. In: Proceedings of Sixth International Symposium on Transport Phenomena and Dynamics of Rotating Machinery, vol. 2. pp. 509–518.

Nakabe, K., Inaoka, K., Ai, T., Suzuki, K., 1996. An experimental study on the flow and heat transfer characteristics of longitudinal vortices induced by an inclined impinging jet into a crossflow. In: Proceedings of Third KSME-JSME Thermal Engineering Conference, vol. 3. pp. 59–64.

Nakabe, K., Inaoka, K., Ai, T., Suzuki, K., 1997. Flow visualization of longitudinal vortices induced byan inclined impinging jet in a crossflow – Effective cooling of high temperature gas turbine blades. Energy Conversions and Managements 38, 1145–1153.

Nakabe, K., Inaoka, K., Higashio, A., Chen, W., Suzuki, K., Kim, J.H., 1998. An experimental study on the flow and heat transfer characteristics of longitudinal vortices induced by an inclined impinging jet into acrossflow (Measurements of heat transfer coefficients using thermochromic liquid crystal). In: Proceedings of 11th International Heat Transfer Conference (to be submitted).

Sparrow, E.M., Goldstein, R.J., Rouf, M.A., 1975. Effect of nozzle – Surface separation distance onimpingement heat transfer for a jet in a crossflow. Trans. ASME: J. Heat Transfer 97, 528–533.

Suzuki, K., 1996. Flow modification and heat transfer enhancement with vortices. In: Proceedings of Ninth International Symposium on Transport Phenomena in Thermal-Fluid Engineering, I. pp. 72–83.

Suzuki, K. et al., 1996. Flow control and heat transfer enhancement with vortices. In: Proceedings of Symposium on Vortices and Heat Transfer. Bochum (in printing).

Tiggelbeck, St., Mitra, N.K., Fiebig, M., 1994. Comparison of wing-type vortex generators for heat transfer enhancement in channel flows. Trans. ASME: J. Heat Transfer 116, 880–885.